한국공작기계기술학회 '97년도 추계학술대회 논문집 pp 132~139

단섬유 금속복합재료의 응력-변형률 히스테리시스 거동 해석

Analysis of Stress-Strain Hysteresis Behavior in Metal Matrix Composites

김홍건*, 전오성 (전주대학교 기계공학과), 최금호(국립기술품질원)

Hong Gun Kim* and Oh Sung Jun (Department of Mechanical Engineering, Jeonju University)
Gum Ho Choe (National Institute for Technology and Quality)

Abstract

The strengthening mechanism of short fiber or whisker reinforced metal matrix composites has been studied by a continuum mechanics treatment utilizing finite element analysis (FEA). To assess the tensile and compressive constitutive responses, a *constraint-unconstraint* comparative study based on stress-strain hysteresis loop has been performed. For analysis procedures, the aligned axisymmetric single fiber model and the stress grouping technique have been implemented to evaluate the domain-based field quantities. Results indicated that the development of significant triaxial stresses within the matrix both for the tensile and compressive loading, due to the constraint imposed by reinforcements, provides an important contribution to strengthening. It was also found that fiber stresses are not only sensitive to the fiber/fiber interaction effects but also substantially contribute to the composite strengthening both for the tensile and compressive loading.

1. Introduction

In recent years, Short Fiber Reinforced Metal Matrix Composites have been extensively investigated because it is more economical to produce economic production of SiC fibers (whiskers), which has also led to the use of platelet, or particulate SiC in MMCs. One of the advantages of discontinuous composite is that they can be shaped by standard metallurgical processes such as forging, rolling, extrusion, and so forth.[1-3]

In MMCs, a thorough evaluation of the merits of various arguments for strengthening in MMCs is often difficult because of the paucity of complete information on the processing, characterization, and properties of the materials. The first and second theories provide approximate predictions of composite response.

On the other hand, some theories of composite strengthening have been proposed that directly relate the composite yield strength to the yield strength of the matrix. Enhanced dislocation density in the matrix of the reinforced alloys is related to the observations of a high density of dislocations generated in the composite matrix during cooling from the processing temperatures due to a difference in the coefficient of thermal expansion between the fiber and matrix.[4-7] The load transfer mechanism between the fiber and matrix also relates to the composite yield strength and predicts that the composite strength is linearly related to the matrix yield strength.[8,9] Here, the composite yield strength is taken to be the 0.2% yield strength. However, since the composite stress-strain curve is typically rather smooth, characterization of the stress-strain response in terms of a yield strength is incomplete. It should also be noted that the *yield strength value* is sensitive to the precise definition of composite yielding.

Further, it would be expected that the difference in

dislocation densities be reflected in an increase in microhardness values for the reinforced matrix material.[4,10] However, this is not observed experimentally for the 2124 SiC whisker composite system where the range of microhardness values for the composite matrix is roughly the same as that of the control alloy.[11] Also, in a SiC particulate reinforced Al-4% Cu composite system, the microhardness value of a peak aged matrix was found to decrease with increasing volume fraction of the reinforcement, despite significant increases in the measured yield strength of the composite.[11]

Residual stresses due to thermal mismatch between the components were proposed as one of the contributors of strengthening mechanism.[12,13] However, it has been presented that the residual stress effects do not make a significant difference in the overall constitutive responses.[14,15] Furthermore, the localized high dislocation densities would result in a work hardened matrix which may be more susceptible to the subsequent deformation and failure.[16]

Finally, the strengthening mechanism arising from constrained plastic flow has been investigated for the composite tensile behavior. In their studies, it was reported that the constrained plastic flow generates the Triaxiality in the matrix so that the role of matrix is significant more than any other factors. However, Kim[16] suggested that the role of fiber may be the major contributor for composite strengthening through the analysis of tensile stress-strain behavior. It seems important to understand that the results of unconstrained representative volume element (RVE) is not realistic as reported in the previous study.[14,15] Thus far, a comparative study between constrained and unconstrained model must give an insight from where the composite strengthening stems.

In this paper, therefore, an attempt to characterize the major composite strengthening mechanism in MMCs has been given in detail through a *constraint-unconstraint* comparative study implementing an elastoplastic FEA and stress grouping approach. It was found that this approach provides a rationale through the constitutive characteristics in MMCs. An axisymmetric single fiber model based on incremental plasticity theory using *von* Mises yield criterion and Plandtl-Reuss equations was employed to evaluate both the constrained and unconstrained RVE. A domain-based stress grouping technique was implemented to obtain the stress-strain hysteresis loop that gives the information of tensile and compressive constitutive responses in a designated region. It was found that the contribution of overall matrix is not significant though it generates a source of strengthening. Finally, comparisons with other strengthening theories were discussed in detail.

2. FE Formulation

The FE formulations in this work are centered on the elastoplastic analysis with small strain plasticity theory[17] using an axisymmetric single reinforcement model. To solve nonlinearity, Newton-Raphson method has been implemented in this study. Consistent with small strain theory,

$$\{d\varepsilon^{el}\} = \{d\varepsilon\} - \{d\varepsilon^{pl}\} \quad (1)$$

where $\{d\varepsilon\}$, $\{d\varepsilon^{el}\}$, and $\{d\varepsilon^{pl}\}$ are changes in total, elastic, and plastic strain vectors, respectively. Elastoplastic stress-strain matrix can be solved iteratively, in which the elastic strain vector is updated at each iteration, and the element tangent matrix is also updated. For a static analysis, the FE discretization process yields a set of simultaneous equations. Finally, *associated* flow rule (Plandtl-Reuss equation) and isotropic hardening rule have been implemented in this study. Further detailed procedures are well described in the previous paper.[18,19]

3. Model and Material

3.1 Model

The micromechanical model to describe a short fiber reinforced composite is an axisymmetric single fiber RVE. In the present model, a uniform fiber distribution with an end gap value equal to transverse spacing between fibers was selected as has been done by Kim.[18,19] The fibers were assumed as uniaxially aligned with no fiber/matrix debonding allowed for, in keeping with the actual situation in many MMCs. With

respect to fiber alignment, Takao, Chou, and Taya[20] concluded that a misorientation angle of less than 10° has little effect on the composite stiffness, while a misorientation angle greater than 15° ~ 20° has a great effect. Quantitative measurement of the fiber misorientation of this material were not made, but visual observations confirmed that the extrusion process has caused a high degree of fiber alignment. In the previous work,[14] the longitudinal and transverse predictions of the FE models were compared to experimental measurements of longitudinal properties, and it was concluded that the effects of fiber misorientation were not of first order significance for the samples. The constraint boundary condition enforces elastic and plastic constraint by requiring that the radial and axial boundary of RVE is maintained in the straight manner during deformation.

On the other hand, the concept of volume average method has been implemented to produce the domain-based stress-strain responses. The overall stress in a domain can be calculated through a simple averaging scheme given by the following equation

$$\langle \sigma_{ij} \rangle_{\Omega} = \frac{\int_{\Omega} (\sigma_{ij})_k \, V_k \, d\Omega}{\int_{\Omega} V_k \, d\Omega} \qquad (2)$$

where $(\sigma_{ij})_k$ is the stress in element k and V_k is the volume of that element. Hence, equation (2) is used to group each domain stress. Hence, the average stress-strain response can be obtained in each domain, which represents regional RVE stresses. By employing this stress grouping approach, a representative domain stress-strain curve can be delineated. In a short fiber reinforced composite, the composite domain Ω_c can be decomposed into the fiber region Ω_f and the matrix region Ω_m as shown in Fig. 2. In the same fashion, the field quantity in the matrix region Ω_m can also be decomposed to the surrounding matrix region Ω_{m1} and the matrix region between fiber ends Ω_{m2} as shown in Fig. 2. This stress grouping is, actually, based on the additionally generated stress components under uniaxial loading due to constraint condition, of which rationale is explained as follows.

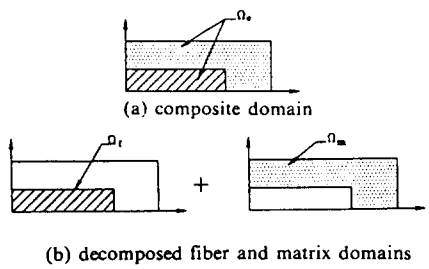

Fig. 1 A schematic of stress grouping approach in a short fiber reinforced composite.(a)composite domain,(b)decomposed fiber and matrix domain.

Figs. 3(a) and (b) show the schematic of deformed shape with and without constraint case. In the unconstrained model shown in Fig 3(a), which has a traction free side wall, the fiber end region is more deformed radially and tangentially than that of the side wall constrained case. In domains of Ω_f, Ω_{m1} and Ω_{m2}, presumably, additional stresses are produced due to constraint effects. In domains of Ω_f and Ω_{m1}, compressive radial and hoop stresses are generated, whereas additional tensile radial and hoop stresses in Ω_{m2} are produced as shown in Fig. 3(b). Note that, the domain boundaries of Ω_{m1} and Ω_{m2} should not exactly be a straight line from the fiber tip but a little shifted presumably. However, grouping of Ω_{m1} and Ω_{m2} provides a general feature of constraint effects. Thus far, stress grouping was intended to analyse domains of Ω_f, Ω_m, Ω_{m1} and Ω_{m2} so as to compare field quantities of the constraint case to those of the unconstraint case.

3.2 Materials

The experimental monotonic tensile stress-strain curves for Al 2124 and Al 2124 reinforced by 20 vol. % SiC fiber were performed using strain controlled tensile test at the strain rate of 10^{-3}/sec in an Instron 1330 Servo-Hydraulic test machine.

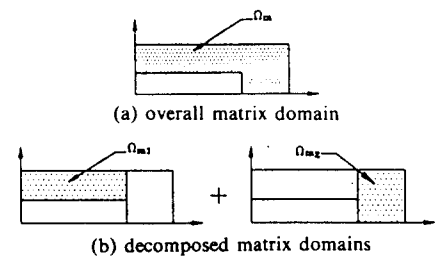

Fig. 2 A schematic of stress grouping approach in the matrix. (a) overall matrix domain, (b) decomposed matrix domains.

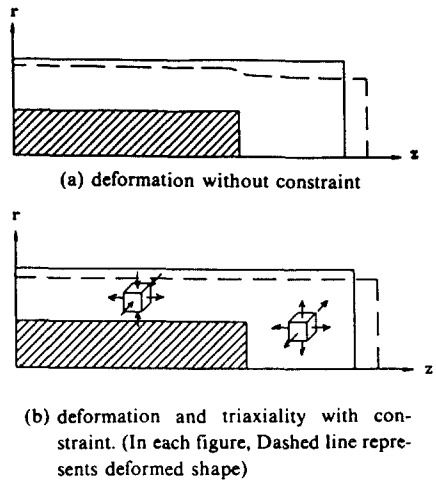

(b) deformation and triaxiality with constraint. (In each figure, Dashed line represents deformed shape)

Fig. 3 A schematic of deformed shape with and without constraint. (a) deformation without constraint, (b) deformation and triaxiality with constraint. (In each figure, Dashed line represents deformed shape).

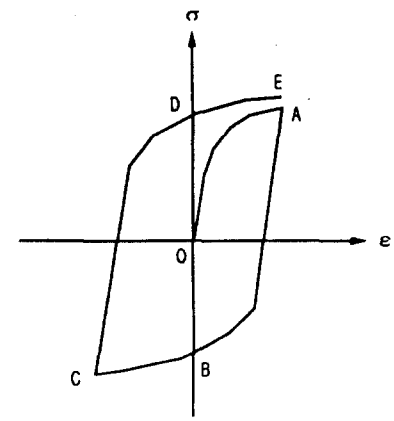

Fig. 4 A schematic of stress-strain hysteresis loop.

The unreinforced Al 2124 was processed in identical fashion to the composite, namely, by a powder metallurgy process involving hot processing above the solidus followed by hot extrusion. The SiC fibers are approximately 1 μm in diameter with an average aspect ratio of 4 and tend to be aligned in the extrusion direction which corresponds to the longitudinal axis of the tensile samples. After machining, the samples were heat treated for T-6 condition. All tensile tests were performed in accordance with the ASTM standard test method, *Tension testing of metallic materials* (ASTM E-8).

From the matrix test data, a bilinear representation of the matrix stress-strain curve was used for computer simulation. Thus, the stress-strain characteristics of the matrix are defined by the elastic modulus, yield stress and work hardening rate (tangent modulus). These characteristics were measured at room temperature on the PM 2124 Al alloy and were found to be E_m=70*GPa*, σ_{my}=336MPa and E_T=1.04GPa, respectively. Other material properties selected are ν_m=0.33 for matrix and E_f=480*GPa*, ν_f=0.17 for reinforcement.[19] Here, E is Young's modulus, E_T is tangent modulus, σ_{my} is matrix yield stress and ν is Poisson's ratio.

The fiber and matrix materials were assumed to be isotropic and the elastic constants are assumed to be temperature independent. The experimental data for compressive stress-strain curves was not needed for input data because the isotropic hardening rule was implemented in this study. Further, thermally induced residual stresses were neglected and these computations are to be performed in the subsequent work.

4. Results and Discussion

4.1 Composite Behavior

To obtain the stress-strain hysteresis behavior numerically, the applied far field strain ε_c was subsequently loaded from 0% (Origin) to 1% (point A), 1% to 0% (point B), 0% to -1% (point C), -1% to 0% (point D), and 0% to 1% (point E), as described in Fig. 4. To solve nonlinear analysis, 25 small load steps of which step has maximum 20 iterations were used incrementally by $\Delta\varepsilon_c$=0.04%. The calculated hysteresis loops of five cycles for isotropic matrix are shown in Fig. 5. The result shows that isotropic matrix was nearly saturated to the matrix ultimate tensile strength

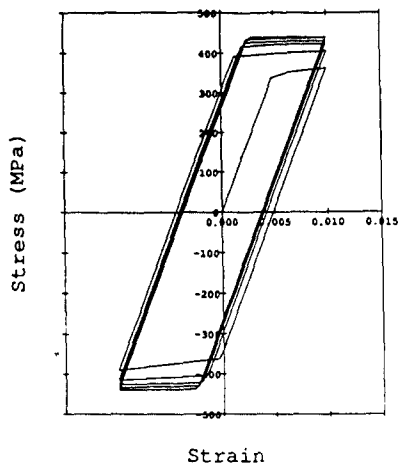

Fig. 5 Calculated hysteresis loops of five cycles for isotropic matrix.

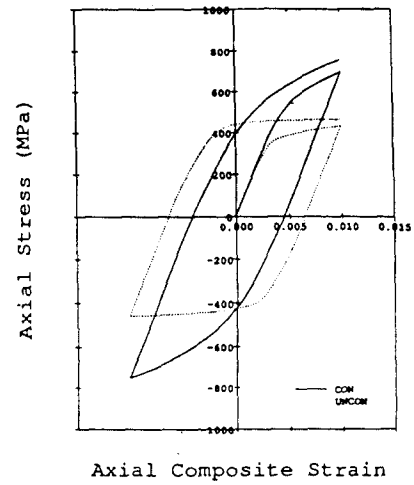

Fig. 6 Numerically predicted stress-strain responses for fully reversed loading between far-field composite strains of 1% and -1% with and without constraint conditions.

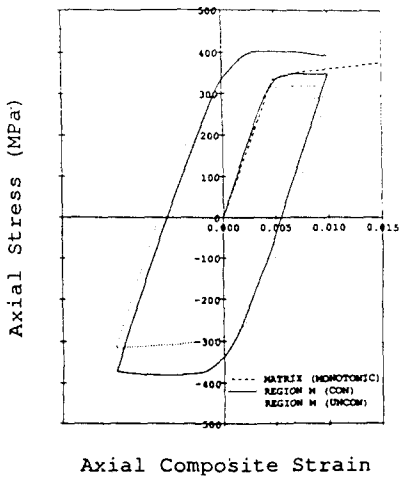

Fig. 7 Total matrix average axial stresses for a hysteresis loop with and without constraint conditions.

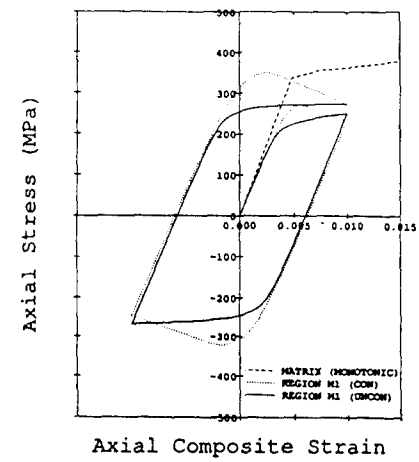

Fig. 8 Decomposed matrix average axial stresses in the region of Ω_{mI} for a hysteresis loop with and without constraint conditions.

even in five cycles. This behavior gives a verification of the program and the theory.

Fig. 6 shows the composite stress-strain hysteresis loop with and without constraint conditions. The tensile and compressive stress-strain behavior of each curve shows a similar fashion as expected. However, it is shown that both loops make a functional difference in the flow regime. The unconstrained RVE shows a little composite strengthening effect, which is the unrealistic constitutive behavior as discussed in the monotonic tensile loading case.[18]

4.2 Role of Matrix

Fig. 7 shows a decomposed matrix stress-strain relation using stress grouping approach. A slight difference between the constrained and unconstrained RVE is shown for the overall matrix strength.

It suggests that fiber/fiber interactions affect to the matrix strength in a domain dependent manner. Therefore, it is inferred that the composite strengthening does not stem from the matrix directly though it generates the factor to enhance the strength.

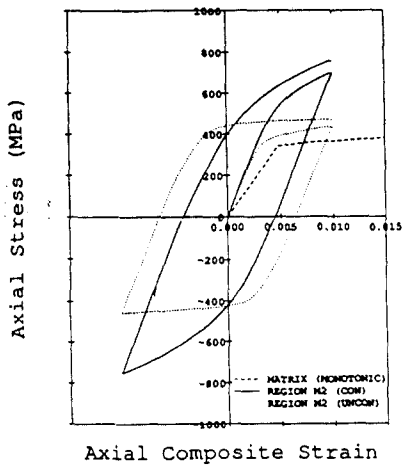

Fig. 9 Decomposed matrix average axial stresses in the region of Ω_{m2} for a hysteresis loop with and without constraint conditions.

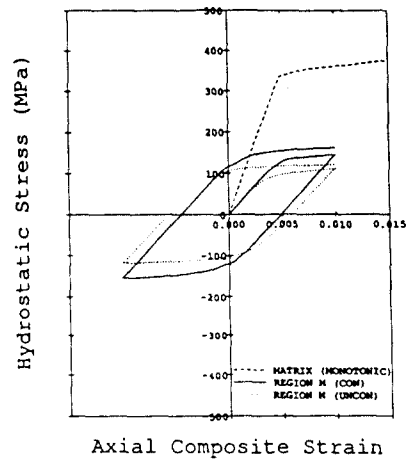

Fig. 10 Total matrix average hydrostatic stresses for a hysteresis loop with and without constraint conditions.

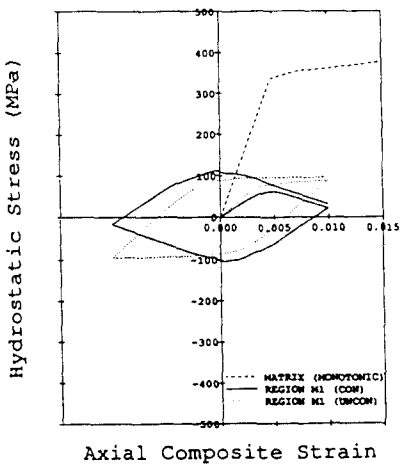

Fig. 11 Decomposed matrix average hydrostatic stresses in the region of Ω_{m1} for a hysteresis loop with and without constraint conditions.

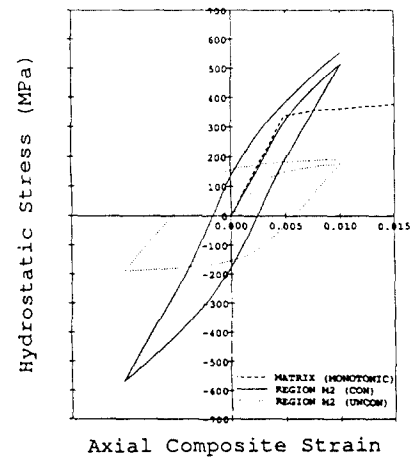

Fig. 12 Decomposed matrix average hydrostatic stresses in the region of Ω_{m2} for a hysteresis loop with and without constraint conditions.

Accordingly, matrix region Ω_m has been divided into Ω_{m1} and Ω_{m2} as described in Fig. 2. Hence, some difference of constraint effect is shown in the domain Ω_{m1} (*see* Fig. 8) whereas the pronounced difference is shown in the domain Ω_{m2} (*see* Fig. 9). Therefore, it is inferred that the constraint condition influences in the domain Ω_{m2} substantially compared to the domain Ω_{m2}. Interestingly, the results of domains of Ω_c and Ω_{m2} show the same values as they should (*see* Figs. 6 and 9). In axisymmetry, the sectional equilibrium condition is required in the axial plane. Thus, the results of homogeneous Ω_{m2} domain must follow the composite behavior.

Matrix hydrostatic stress-strain hysteresis loops in the domains of Ω_m, Ω_{m1}, and Ω_{m2} for the constrained and unconstrained RVEs are shown in Figs. 10 to 13, respectively. In the domains of Ω_m and Ω_{m1}, however, the pronounced constraint effects on hydrostatic stresses are not shown, whereas hydrostatic stresses in domain Ω_{m2} show markedly high values because of the additionally generated tensile triaxiality for the constrained RVE.

This enhancement of hydrostatic stresses results in the expansion of yield surface, which prohibits the

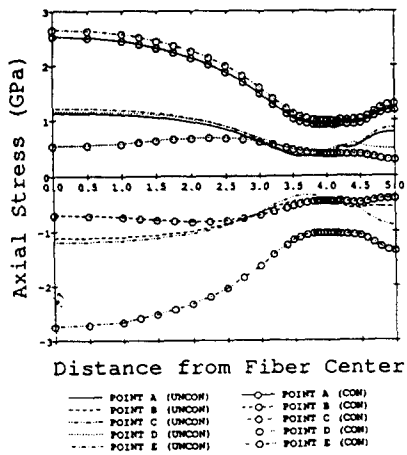

Fig. 14 Fiber stresses on the center line as a function of distance normalized by fiber radius with and without constraint conditions.

extensive plastic deformation. On the contrary, hydrostatic stresses in the domain Ω_{ml} for the constrained RVE decrease as the far field load increases due to the additionally generated opposite radial stress component. Thus far, the resulting matrix hydrostatic stress for the constrained RVE shows slightly higher values than that of the unconstrained RVE. It is found that the pronounced constraint effects on hydrostatic stresses stem from the additionally generated tensile triaxiality.

4.3 Role of Fiber

Fig. 13 describes the fiber stresses at five points (A, B, C, D, and E) on the hysteresis loop. Note that the points located were explained in the previous section. The fiber average axial stresses of the unconstrained RVE indicate that the fiber stresses are quite limited. At the unloaded state (ε_c=0%), such as points B and D, it is shown that the substantial fiber stresses are remaining due to the plasticity in the matrix. Likewise, the constrained RVE also shows some stresses at the unloaded state though the magnitude is not so high. Further, the fiber stresses of constrained RVE are well over 2 GPa at 1% far field composite strain. The implication of this result indicates that the major composite strengthening mechanism stems from fiber strengthening generated by sectional equilibrium in the axial direction based on tensile triaxiality. The high fiber stress intensification is important from the standpoint of potential fiber fracture during the deformation of MMCs. Preliminary results[21] suggest that the fiber actually fracture during tensile straining of MMCs.

5. Conclusions

The constitutive characteristics of MMCs were studied numerically with the objective of investigating the tensile and compressive composite behavior and the major strengthening contributor. By means of the stress grouping approach, a *constraint-unconstraint* comparative study based on stress-strain hysteresis loop was performed and several sequences with key elements of strengthening were identified. It was found that the constrained plastic flow and triaxiality in the matrix gives a substantial contribution of composite strengthening both for the tensile and compressive loading.

Acknowledgements

This work has been performed by the preliminary study for "Structural analysis for the large capacity automatic monorail transportation system". Authors greatly appreciate Sunjin Co. for this grant.

References

[1] Divecha, A. P., Fishman, S. G. and Karmarkar, S. D., "Silicon Carbide Reinforced Alumunum - A Formable Composite," Journal of Metals, pp. 12-17 (1981).

[2] Vogelsang, M., Arsenault, R. J. and Fisher, R. M., "An In-Situ HVEM Study of Dislocation Generation at Al/SiC Interfaces in Metal Matrix Composites," Metallurgical Transactions A, Vol. 17A, pp. 379-388 (1986).

[3] Gibson, R. A., "Principles of Composite Material Mechanics," pp. 156-189, McGraw-Hill Inc. (1994).

[4] Arsenault, R. J. and Fisher, R. M., "Microstructure of Fiber and Particulate SiC in Al6061 Composite," Scripta Metallurgica, Vol. 17, pp. 67-71 (1983).

[5] Taya, M. and Arsenault, R. J., "Metal Matrix Composites, Thermomechanical Behavior," pp. 1-8, Pergamon Press, NY (1989).

[6] Arsenault, R. J. and Shi, N., 1986, "Dislocation Generation Due to Differences between the Coefficients of Thermal Expansion," Materials Science and Engineering, Vol. 81, pp. 175-187.

[7] Taya, M. and Mori, T., 1987, "Dislocations Punched-Out around a Short Fiber Metal Matrix Composite Subjected to Uniform Temperature Change," Acta Metallurgica, Vol. 35, No. 1, pp. 155-162.

[8] Nardone, V. C., 1987, "Assessment of Models Used to Predict the Strength of Discontinuous Silicon Carbide Reinforced Aluminum Alloys," Scripta Metallurgica, Vol. 21, pp. 1313-1318.

[9] Nardone, V. C. and Prewo, K. M., 1986, "On the Strength of Discontinuous Silicon Carbide Reinforced Aluminum Composites," Scripta Metallurgica, Vol. 20, pp. 43-48.

[10] Arsenault, R. J., 1984, "The Strengthening of Aluminum Alloy 6061 by Fiber and Platelet Silicon Carbide," Materials Science and Engineering, Vol. 64, pp. 171-181.

[11] Christman, T., Needleman, A. and Suresh, S., 1989, "An Experimental and Numerical Study of Deformation in Metal-Ceramic Composites," Acta Metallurgica, Vol. 37, No. 11, pp. 3029-3050.

[12] Koss, D. A. and Copley, S. M., 1971, "Thermally Induced Residual Stresses in Eutectic Composite," Metallurgical Transactions, Vol. 2, pp. 1557-1560.

[13] Arsenault, R. J. and Taya, M., 1987, "Thermal Residual Stress in Metal Matrix Composite," Acta Metallurgica, Vol. 35, pp. 650-659.

[14] Levy, A and Papazian, J. M., 1991, "Elastoplastic Finite Element Analysis of Short Fiber Reinforced SiC/Al Composites: Effects of Thermal Treatments, " Acta Metallurgica, Vol. 39, No. 10, pp. 2255-2266.

[15] Nair, S. V. and Kim, H. G., 1991, "Thermal Residual Stress Effects on Constitutive Response of a Short Fiber or Whisker Reinforced Metal Matrix Composite," Scripta Metallurgica, Vol. 25, No. 10, pp. 2359-2364.

[16] Kim, H. G., 1992, "Micromechanics of Deformation in Short Fiber or Whisker Reinforced Metal Matrix Composites," Ph.D Dissertation, Department of Mechanical Engineering, University of Massachusetts, Amherst, MA, USA.

[17] Cook, R. D., Malkua, D. S. and Plesha, M. E., 1989, "Concepts and Applications of Finite Element Analysis," John Wiley and Sons, Third Edition, pp. 163-295.

[18] Kim, H. G., 1994, "Assessment of Plastic Constraint Effects Induced by Whisker Interactions in Whisker Reinforced Metal Matrix Composites," Journal of the Korean Society for Composite Materials, Vol. 7, No. 3, pp. 1-10.

[19] Kim, H. G., 1994, "Stress Transfer in Shear Deformable Discontinuous Composites," KSME Journal, Vol. 8, No. 4, pp. 475-484.

[20] Takao, Y., Chou, T. and Taya, M., 1982, "Effective Longitudinal Young's Modulus of Misoriented Short Fiber Composites," Journal of Applied Mechanics, Vol. 49, pp. 536-540.

[21] Murdeshwar, N., 1989, "Fracture Development in a 20 Volume Percent Silicon Carbide Whisker Reinforced Al 2124 Metal Matrix Composite," M. S. Thesis, University of Massachusetts at Amherst, MA, USA.

[22] Cho, K. and Gurland, J., 1988, Metallurgical Transactions, Vol. 19A, pp. 2027.